

Visualization of origins and propagation of excitation in canine gastric smooth muscle

RANDEL J. STEVENS, JEFFERY S. WEINERT, AND NELSON G. PUBLICOVER
*Biomedical Engineering Program, Department of Physiology and Cell Biology,
University of Nevada School of Medicine, Reno, Nevada 89557*

Stevens, Randel J., Jeffery S. Weinert, and Nelson G. Publicover. Visualization of origins and propagation of excitation in canine gastric smooth muscle. *Am. J. Physiol.* 277 (*Cell Physiol.* 46): C448–C460, 1999.—The origin and spread of excitation were visualized with fluo 3 fluorescence in tissues isolated from canine gastric antrum. Sheets of circular muscle (5 × 6 mm) had at least 1 (30%) and up to 3 discrete slow-wave pacing sites located near the longitudinal-circular muscle boundary, whereas similarly sized longitudinal sheets had an average of 5 sites (range 3–12 sites) that initiated Ca²⁺ waves. Superimposed fluorescent oscillations (circular muscle) and spikes (longitudinal muscle) were seen to initiate and propagate as distinct events, separate from their underlying activities. Average propagation velocities transverse (6–7 mm/s) and parallel (39–45 mm/s) to the long axis of muscle fibers were similar for each type of event in circular and longitudinal tissues; however, distinct regions where velocities of some (but not all) events decreased by up to an order of magnitude were present. The distance propagated by individual events was limited by collisions with concurrent excitable events or recently activated regions. Complex patterns of excitation in gastrointestinal smooth muscle arise as a result of interactions between multiple pacing sites, heterogeneous conduction velocities, and the interplay of adjacent pacemaker domains.

electrophysiology; calcium; fluorescence

GASTRIC PERISTALSIS occurs when slow waves originating near the greater curvature of the corpus propagate aborally toward the pylorus (4, 12, 32). At the cellular level, the strength of peristaltic contractions is influenced by the degree of slow-wave depolarization (5) and the coexistence of other excitable events such as spike-like action potentials (12) and superimposed oscillations in membrane potential (5, 12, 37). However, the overall efficacy of peristalsis can be affected by a number of additional factors including the locations of pacemaker activity (1, 32), the spontaneous frequencies at each site (13), the synchronization of sites, the excitation conduction velocities in each axis, and the distances traveled in each direction (25). Although considerable progress toward understanding the membrane and intracellular pathways that regulate cellular excitability has been made (3, 10, 17), less is known about intercellular interactions that affect the coordination of peristalsis. In this study, the origin and propagation of excitation in gastric tissue segments were directly observed by low-light, fluorescent video techniques.

The costs of publication of this article were defrayed in part by the payment of page charges. The article must therefore be hereby marked "advertisement" in accordance with 18 U.S.C. Section 1734 solely to indicate this fact.

Most studies of the origin and propagation of excitation in smooth muscle have employed multiple electrodes to detect arrival times of electrical activity in isolated tissue segments. Early studies using extracellular electrodes suggest that complex synchronized spikes of electrical activity arise from the summation of functional muscle units and not individual muscle fibers (2). These studies also demonstrate that conduction velocities in the long axis of muscle fibers are ~10 times greater than those found in transverse directions (21). By measuring arrival times at two intracellular micropipettes in cross-sectional preparations, Bauer and his colleagues (1) were the first to suggest on the basis of electrophysiological evidence that gastric slow waves originate in the circular layer region near the myenteric border, although Thuneberg (36) had earlier reached this conclusion on the basis of morphological data. The existence of so-called "hot-spots" or preferred locations in tissues where the majority of slow waves originate was demonstrated by using triangulation algorithms and event arrival times at three intracellular microelectrodes (28). In each of these studies, it has been assumed that unitary events emerge and propagate via direct pathways with uniform conduction velocities throughout tissue segments (26). Although these techniques provide estimates of pacing locations and their variability, the presence of muscle bundles (6), septal structures (38), different cell types, and other inhomogeneities (7, 23) suggests that propagation velocities and pathways may not be uniform.

More recently, Lammers and his colleagues (13, 14) employed an array of 240 extracellular surface electrodes covering an area of 15 × 16 mm to investigate the propagation of slow waves in the rat myometrium (14) and rabbit duodenum (13). They developed "isochrones" (contour maps indicating wave fronts at specific times) in order to show the progression of electrical events. These maps provided some of the first evidence of the complexity of conduction patterns and pathways in smooth muscle, although the ability to accurately identify the origin and exact pathways of individual events was somewhat limited by the spatial resolution of the recording system (1 mm).

In the present study, the origin, propagation velocities, conduction pathways, and extent that Ca²⁺ waves propagate in circular and longitudinal muscle layers of the stomach were visualized. Video sequences demonstrate that complex interactions among tissue regions arise as a result of Ca²⁺ waves emerging from multiple pacing sites. Ca²⁺ transients associated with slow waves in circular and longitudinal muscles, oscillations in fluorescence superimposed during slow waves in circular muscle, and rapid spikelike changes in fluores-

cence superimposed during slow waves in longitudinal muscle each originate as unitary events from discrete locations. Excitation patterns are also influenced by temporally and spatially inhomogeneous conduction velocities, collisions of events, morphological boundaries, and tissue injury.

METHODS

Muscle preparation. Mongrel dogs of either sex were killed with pentobarbital sodium (30 mg/kg body wt). After the abdomen was opened, the entire stomach was removed and placed in a bath containing Krebs-Ringer bicarbonate (KRB) solution. Sheets of muscularis from the ventral surface, 7–9 cm oral to the pyloric sphincter, were removed from the underlying mucosa. In some experiments, the muscularis was dissected to expose a cross-sectional preparation (12 × 4 mm) containing both muscle layers as previously described (1). In other experiments, strips (16 × 10 mm) were carefully dissected to form sheets of tissue consisting of either longitudinal or circular muscle.

The general procedure to load the Ca²⁺-sensitive dye fluo 3 and record fluorescence in these tissues has been reported previously (22). Briefly, muscles were placed in 35-mm petri dishes and allowed to equilibrate for 2–3 h in KRB at 37°C. The bottoms of dishes were replaced with thin (no. 1) glass coverslips and coated with a clear resin (Sylgard; Dow Corning). Tissues were pinned rigidly to reduce any movement artifact. Preparations were treated with 5 × 10⁻⁶ M fluo 3-AM, 0.01% DMSO, and 0.025% noncytotoxic detergent cremophor EL for 35–45 min. When dye loading was complete, muscle strips were allowed to equilibrate for an additional 15 min at 37°C in KRB before use.

Data acquisition. Muscle strips were illuminated at 470 ± 20 nm, and fluorescent signals >510 nm were recorded as a measure of excitation. Unloaded tissues produced no significant changes in fluorescence during rhythmic contractile activity. Although fluo 3 (when used alone) does not provide an opportunity to perform ratiometric calibration, increases in fluorescence likely result from increases in cytosolic Ca²⁺ concentration ([Ca²⁺]_i). We have previously reported increases in [Ca²⁺]_i associated with slow waves in these tissues by using the ratiometric dye indo 1 (22). Fluorescent signals were collected with an intensified video camera (Hamamatsu C1966 type 20 or Dage-MTI model SIT-66X) attached to the video port of an inverted epifluorescence microscope (Nikon Diaphot). Images were stored on a computer-controlled videocassette recorder (Sanyo model GVR-S950) at a rate of 30 frames/s.

The microscope was modified to include a platform (custom built) to stabilize a micromanipulator (Narishige model MM-3) suitable for intracellular recordings. Cells were impaled with glass microelectrodes filled with 3 M KCl having resistances in the range of 30–50 MΩ. Transmembrane potentials were measured by a standard, high-impedance electrometer (World Precision Instruments model 7000). The same micromanipulator was used to lower “broken” unfilled glass microelectrodes (tip diameter up to 0.2 mm) onto tissues to explore the effects of localized injuries on pacing sites.

To archive image data while preserving the temporal relationship between transmembrane potentials and fluorescent video signals, membrane potentials were converted to a range of audio frequencies (1–8 kHz) with a custom-designed circuit. A voltage-to-frequency converter (Burr-Brown) allowed membrane potential to be recorded on one audio channel of the videocassette recorder while fluorescent video images were simultaneously recorded. When data were played

back through the videocassette recorder, membrane potential was retrieved with a frequency-to-voltage converter (Burr-Brown). The temporal phase shift introduced by converting a voltage to a frequency-modulated signal and back to a voltage was less than one video frame (33 ms).

Data analysis. Analysis of the video fluorescence signals was performed with both custom-designed and commercially available (Adobe Photoshop) software. Images were digitized (640 × 480 pixels) with a frame grabber (Data Translation model 3152) that has the ability to separately control the gain and offset of the video signal, allowing background light levels to be subtracted before amplification. Membrane potentials were acquired with an analog-to-digital converter (Precision Electronics model PCL-711B). Because each frame on the videocassette recorder could be accessed individually, temporal resolution of video data was 33.3 ms (i.e., 30 frames/s).

To view propagation, series of contrast-enhanced images were computed by storing an initial frame (with no apparent activity) as a “background image.” This image was subtracted from each subsequent frame. An intensity threshold was then applied to each pixel within a frame to enhance contrast. To further aid visualization, all contrast-enhanced frames are displayed as “negative images” in which dark areas indicate regions of increased fluorescence intensity. The net effect of applying a threshold is to make the decision whether the region represented by each pixel is in the excited state (dark) or not (light). No other determinations from the amplitude of fluorescent signals were made [except to display raw summed fluorescence traces (see Figs. 1 and 2) and to note that there was no substantial increase in fluorescence when 2 events “collide”]. Quantitative measurements were restricted to those involving space (e.g., pacing location) or time (e.g., spontaneous frequency at each location) during the initiation, spread, and termination of activity. Conduction velocities were measured by determining the distance traveled by a wave front over each digitized image (i.e., over a 33-ms interval). Statistics are reported as means ± SDs.

Solutions. The KRB used in this study contained (in mM) 137.4 Na⁺, 5.9 K⁺, 2.5 Ca²⁺, 1.2 Mg²⁺, 134 Cl⁻, 15.5 HCO₃⁻, 1.2 H₂PO₄⁻, and 11.5 dextrose (all Fisher Scientific). This solution had a pH of 7.3–7.4 at 37.5°C when bubbled to equilibrium with 97% O₂-3% CO₂. Fluo 3 was purchased from Molecular Probes (Eugene, OR). DMSO, TTX, and cremophor EL were from Sigma (St. Louis, MO).

RESULTS

Types of excitation in smooth muscle. The Ca²⁺-sensitive dye fluo 3 was selected to monitor the origin and propagation of excitation because of its high absorbance (molar extinction coefficient) and low background fluorescence when not bound to Ca²⁺ (8). Excitation of fluo 3 at long wavelengths avoids the intrinsic tissue fluorescence inherent in smooth muscles (22). In addition, because of its dissociation constant (K_d) and high quantum efficiency on Ca²⁺ binding, fluo 3 undergoes a substantial increase in fluorescence intensity over the range of Ca²⁺ levels found in gastrointestinal tissues (22). Because fluo 3 does not directly monitor membrane potential, experiments to establish the relationship between propagated events visualized by fluo 3 fluorescence and those recorded by traditional electrophysiological techniques were performed.

Figure 1A shows an example of the initiation and spread of a typical Ca²⁺ wave recorded from a cross-sectional preparation isolated from the antrum. The

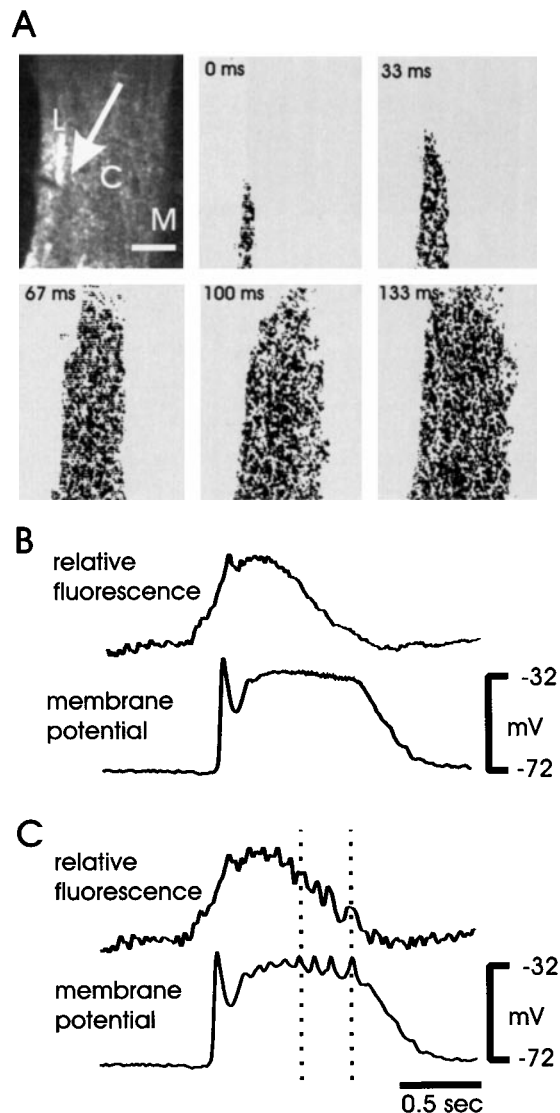


Fig. 1. Types of excitation in circular muscle. *A*, top left: background fluorescent image of cross-sectional preparation showing longitudinal (L), circular (C), and mucosal (M) regions. Contrast-enhanced images (*A*, 0–133 ms) show regions of elevated cytosolic Ca^{2+} concentration ($[\text{Ca}^{2+}]_i$) associated with a slow wave as it emerged near the longitudinal-circular border and propagated throughout entire circular muscle layer. *B* and *C*: intracellular membrane potentials and fluorescence intensities in region of electrode (summed intensities from 9×9 pixels centered on electrode; location indicated by arrow in *A*). Ca^{2+} transients superimposed on some slow waves (*C*) appear as synchronous (dotted lines) oscillations in fluorescence intensity and membrane potential. Scale bar = 2 mm.

frame at *time 0* shows a Ca^{2+} wave emerging within the field of view in the region near the longitudinal-circular muscle boundary. Subsequent frames show rapid spread of the wave front in the direction parallel to the long axis of circular muscle fibers (oriented approximately vertically in the series of images) and slower propagation transverse to this direction. Circular muscle within the entire field of view remained in the excited state throughout the full duration of the slow wave (4 s; individual frames not shown). In cross-sectional preparations, Ca^{2+} waves associated with excitable events in

the circular layer were never observed to spread (above threshold levels) into the longitudinal or mucosal layers.

A myocyte in the circular layer near the longitudinal boundary was impaled with an intracellular microelectrode at the location indicated by the arrow in the background image (see METHODS) in Fig. 1*A*, top left. The upper traces in Fig. 1, *B* and *C*, show summed fluorescence in the immediate region of the impaled cell. The lower traces show electrical slow waves recorded simultaneously from this cell over the same period of time. Circular muscle cells near the longitudinal boundary in dye-loaded and illuminated tissues had resting membrane potentials of -72 ± 5 mV and depolarized to plateau potentials of 31 ± 3 mV with a spontaneous slow-wave frequency of $1.5 \pm 0.5 \text{ min}^{-1}$ ($n = 11$). On the basis of observations of hundreds of slow waves simultaneously recorded with fluorescent images, all slow waves were associated with Ca^{2+} waves that propagated throughout the circular layer, and no Ca^{2+} waves were observed in circular muscle without a concurrent electrical slow wave.

In some cases, fluctuations in fluorescence intensity were superimposed during the plateau phase of a slow wave. These superimposed “oscillations” are discrete events that emerge from multiple sites (not generally the site of origin of the ongoing slow wave) and can be seen in video records to propagate over substantial distances (from <1 mm up to the entire field of view). In Fig. 1*C*, fluctuations appear as small oscillations in summed fluorescence records (upper trace) correlated temporally with oscillations in membrane potential (lower trace). These oscillations are more prominent in tissues removed from distal regions of the stomach (data not shown).

In cross-sectional preparations, the longitudinal muscle layer was generally too thin to accurately track the propagation of excitation. Therefore imaging was performed on sheets of longitudinal muscle (with the circular layer removed) viewed from the serosal side. Figure 2*A* shows an example of the emergence of a Ca^{2+} wave that spreads rapidly parallel to the long axis of the longitudinal fibers (oriented approximately vertically in Fig. 2*A*) and more slowly in the transverse direction to envelop the entire field of view within 133 ms. A myocyte was impaled at the location indicated by the arrow in the background image of Fig. 2*A* (top left). In Fig. 2, *B* and *C*, membrane potentials from this cell are plotted on the same time scale as summed fluorescence intensities from a small region of pixels that included the impaled cell. Preparations had transmembrane potentials of -52 ± 5 mV at the most negative point of voltage excursions and depolarized to 34 ± 5 mV (excluding depolarizations associated with fluorescence spikes; $n = 20$ regions within 8 tissues). Electrical slow waves in longitudinal muscles (as shown in Fig. 2, *B* and *C*) were consistently associated with propagated Ca^{2+} waves in video sequences. When observations of Ca^{2+} transients were isolated to specific locations within a field of view, events were observed at a mean frequency of $15 \pm 3 \text{ min}^{-1}$ ($n = 20$ tissues).

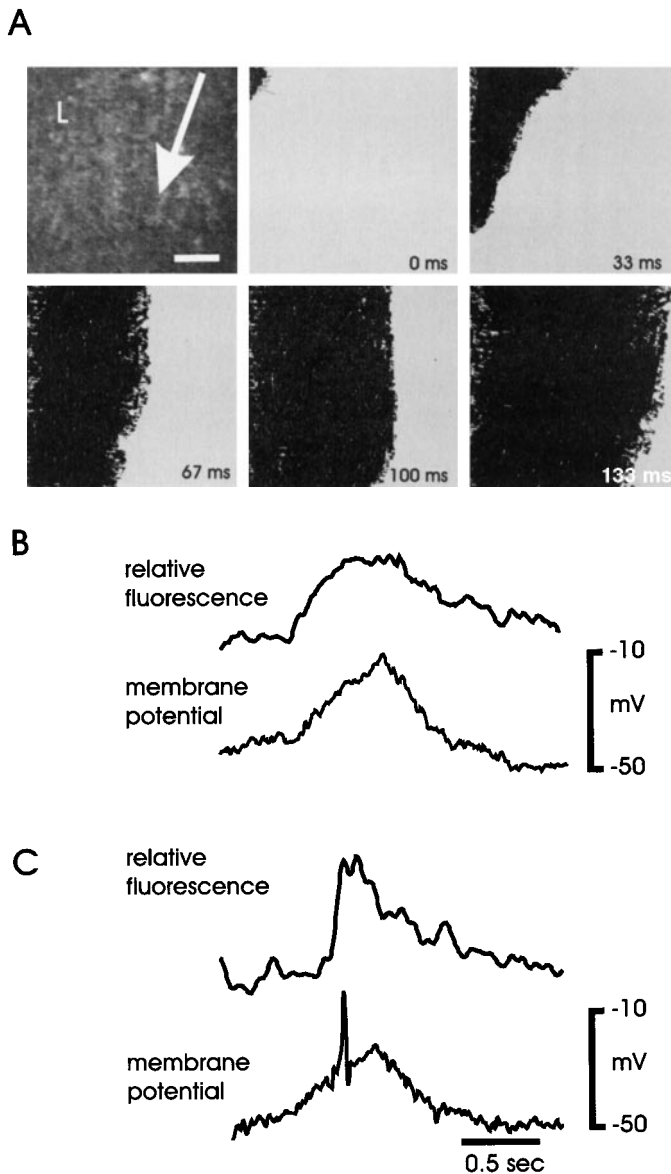


Fig. 2. Types of excitation in longitudinal muscle. A sheet of longitudinal muscle (background frame; *A*, top left) with no circular muscle attached was viewed from the serosal side. Contrast-enhanced images (*A*, 0–133 ms) show propagation of Ca^{2+} transient associated with a longitudinal slow wave. *B* and *C*: comparison of intracellular membrane potentials (electrode location indicated by arrow in *A*) with fluorescent intensities recorded simultaneously in region of electrode (summed intensities from 81 pixels). During some Ca^{2+} waves (*C*), superimposed fluorescent spikes were observed in some cells within region of elevated fluorescence. Scale bar = 2 mm.

The electrical record in Fig. 2*C* is an example in which a spikelike action potential occurred during the slow wave. The action potential was associated with a superimposed sharp rise in fluorescence (upper trace) that could be seen in video images to propagate only over limited distances (<1 mm) within the region of elevated $[\text{Ca}^{2+}]_i$ associated with the slow wave. In stomach, not all preparations produced action potentials superimposed on longitudinal slow waves. In addition, in preparations where action potentials were observed, they were not seen in all sweeps of elevated

fluorescence (observed in 10 of 60 Ca^{2+} sweeps in cells from 10 tissues). In other words, rapid fluctuations in fluorescence superimposed on the elevated Ca^{2+} transient associated with a slow wave were often observed to sweep through the region of a microelectrode impalement without electrical spikelike action potentials from an individual cell being recorded.

Origin of excitation. The nature of the origin of slow waves and whether slow waves are initiated from a single location have been the subject of debate for a number of years (24). Figure 3 shows an example in which the emerging phase of a Ca^{2+} transient associated with a slow wave has been captured in a narrow region along the circular-longitudinal muscle boundary. These frames demonstrate the emergence of a Ca^{2+} wave as a unitary event. If left undisturbed (i.e., without neural blockade or other tissue manipulations), Ca^{2+} waves (associated with electrical slow waves; see Fig. 1*B*) originated from one to three distinct pacemaker locations in circular sheets (6×5 mm) over 30-min observation periods ($n = 12$). In 33% of preparations, a single pacing site was detected. The remaining tissues had two to three distinct sites where at least some events from each site could be observed throughout the observation period.

Similarly sized sheets of longitudinal muscle contained many more spontaneous pacing sites. In 20 tissues viewed over 30 min, there was an average of 5 (range 3–12) distinct pacing locations. Longitudinal sites appeared to be more transient than those in the circular muscle layer. When viewed over prolonged periods (30–60 min), new sites where activity had not previously been observed occasionally appeared while other active sites disappeared. In tissues that were not manipulated throughout the observation period, no causes for the appearance or disappearance of these sites were apparent.

Figure 4 demonstrates the reproducibility of these discrete pacing locations in a longitudinal muscle preparation. The emergence of four contiguous Ca^{2+} waves is shown. The first two Ca^{2+} waves (Fig. 4, *A* and *B*) originated from the same location to within the temporal and spatial resolution of the imaging system (pixel resolution $\sim 16 \mu\text{m}$). The third event (Fig. 4*C*) emerged from a clearly distinct site and was followed by an event (Fig. 4*D*) from the same location as that for the first two events. Individual pacing sites, once established in circular or longitudinal muscle preparations, were not observed to vary (to within the spatial resolution of the imaging system) throughout prolonged observation periods (>30 min). The invariant locations of individual pacing sites were not affected by interspersed events from other sites.

Synchronization of pacemakers. As noted previously, one-third of circular muscle preparations revealed a single pacing site when viewed over an observation period of 30 min. Circular tissues with multiple sites demonstrated periods in which one site might dominate (initiating 50–100% of Ca^{2+} waves) for periods of 5 min or more (up to the 30-min observation period). Then dominance might shift to another site before returning to the initial site. In other words, if an event initiated at

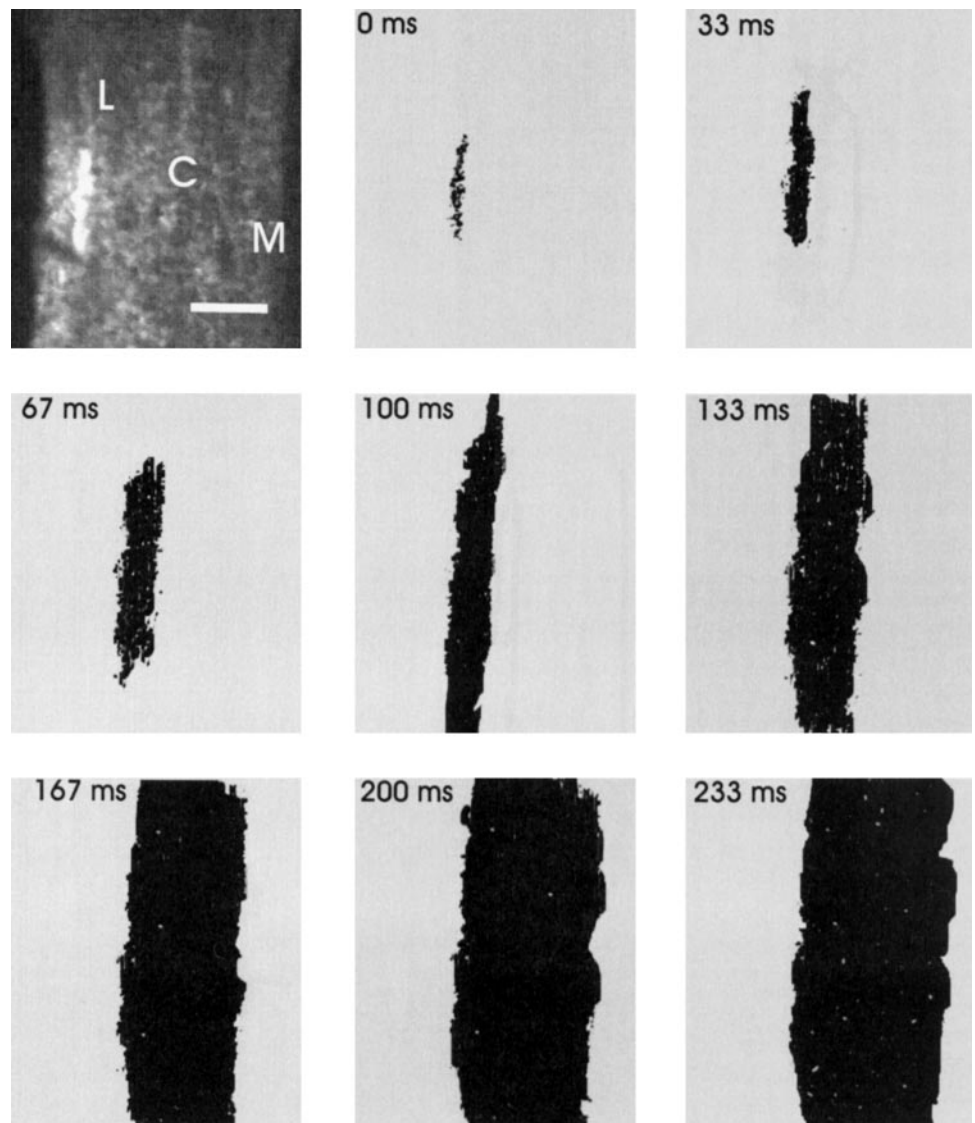


Fig. 3. Ca^{2+} waves in circular muscle arise near circular-longitudinal boundary. *Top left*: background fluorescence image of a cross-sectional preparation showing L, C, and M regions. Contrast-enhanced images show emergence (0 ms) of a Ca^{2+} wave near longitudinal-circular boundary. Propagation of Ca^{2+} wave (up to 233 ms) resulted in a region of elevated $[\text{Ca}^{2+}]_i$ that encompassed entire circular muscle. Scale bar = 2 mm.

one site, the next event was most likely to begin at the same site. Except for this observation, there were no clear patterns of initiation among multiple sites in circular muscle strips.

On the other hand, repeatable patterns of activity from multiple pacing sites in longitudinal muscle preparations were frequently observed. These patterns varied in complexity from two sites initiating alternating events for brief periods to intricate patterns involving numerous sites. An example of complex synchronized activity in the longitudinal layer is illustrated in Table 1. Patterns often showed some variability (as in Table 1); however, the initiation of a new series was often recognized by activity at a pacing site that appeared to initiate the sequence and/or a prolonged delay (lasting up to 2 min) after the previous sequence. There was no correlation between pacing sites with the highest intrinsic frequency and those that initiated repeat patterns.

Conduction velocities. In circular muscle, maximum propagation velocities of Ca^{2+} waves transverse to the long axis of muscle fibers averaged 6.2 ± 3.0 mm/s ($n =$

12 tissues), whereas in longitudinal muscle the average was 7.0 ± 3.0 mm/s ($n = 12$ tissues). At standard 30 frame/s video rates, variations in conduction velocities in the direction of the long axes of muscle fibers could only be assessed over one to three frames. In longitudinal muscle, the average propagation velocity of Ca^{2+} waves in this direction was estimated as 45.0 ± 5.0 mm/s ($n = 6$ tissues). In circular muscle, where propagation distances are generally longer, the mean conduction velocity was 39.0 ± 9.0 mm/s ($n = 12$ tissues). It was difficult to accurately measure the propagation velocities of superimposed activities (fluorescence oscillations and spikes) because of short propagation distances and the need to discriminate wave fronts within fluorescence levels that were already elevated; however, conduction velocities were in the same range as those for the underlying Ca^{2+} waves.

It has previously been shown that slow-wave conduction velocity is dependent on the interval since depolarization during electrically paced activity in circular muscle of the canine antrum (27). Video sequences

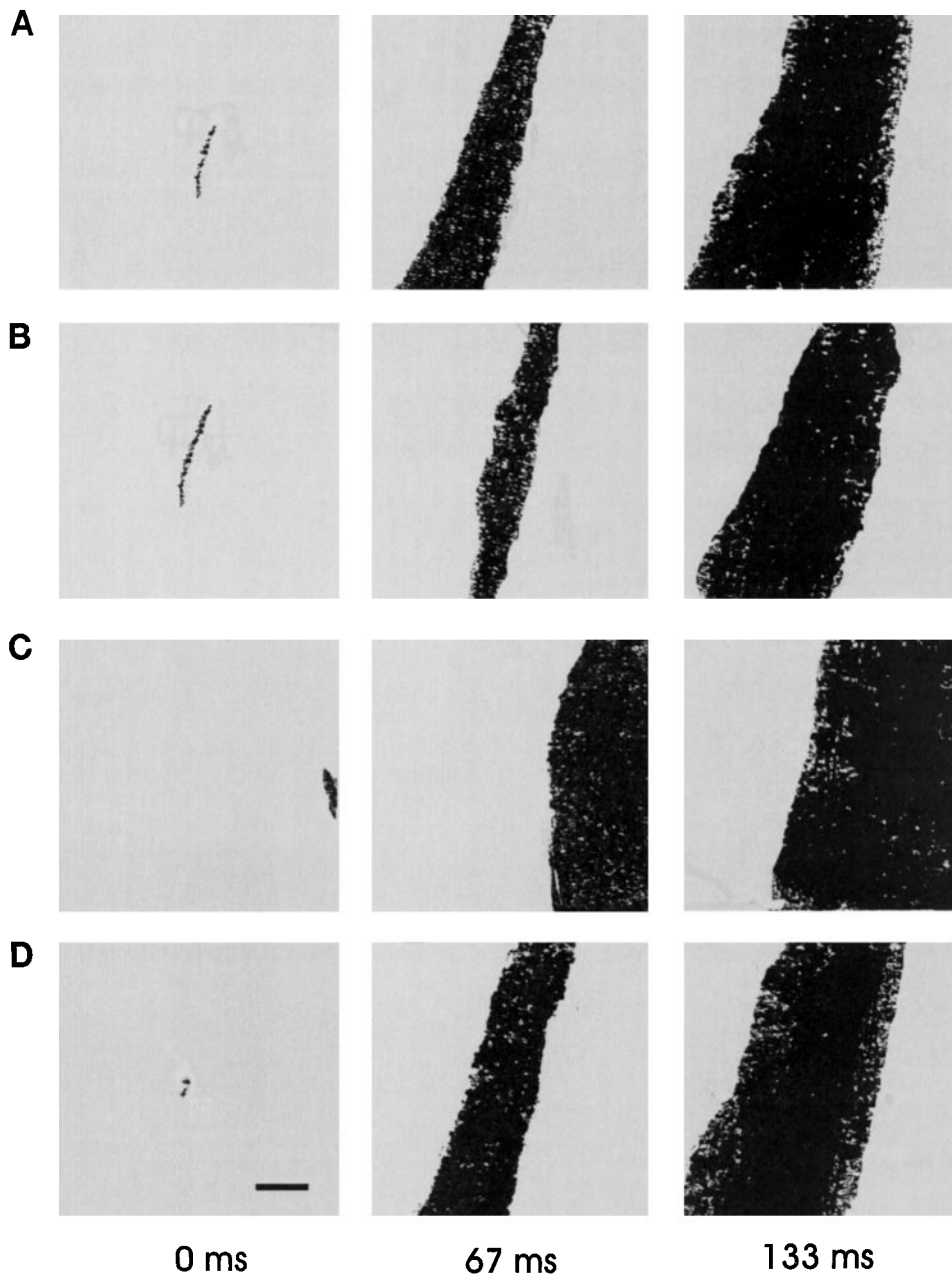


Fig. 4. Repeated activity from longitudinal pacing sites. *A-D*: contrast-enhanced images of 4 contiguous events at 0 (initial event detection), 67, and 133 ms. *A* and *B*: event originating from same site (to within temporal and spatial resolution of imaging system). *C*: event originating from a different site before pacing activity returned to original site (*D*). Slight variations in size of excited region appear at 0 ms because spontaneous generation of events is not synchronized with frame rate (30 frames/s) of camera. Scale bar = 2 mm.

illustrate that this relation is also apparent during spontaneous activity in longitudinal tissues. There is generally insufficient spontaneous variation in slow-wave frequency to readily demonstrate the relation in circular muscle segments; however, longitudinal muscle segments have multiple pacing sites, and most events do not propagate throughout the entire field of view. This results in isolated regions or "islands" within tissues where the interval since depolarization varies substantially. Figure 5 shows an example of conduction velocities measured transverse to the long axis of muscle fibers in regions where spontaneous variations in the interval since the previous depolarization were generated. Although a linear regression has been drawn through these data, there was an upper limit to conduction velocities (i.e., after prolonged intervals).

In addition to temporal variations in conduction velocities, video sequences clearly show discrete spatial regions where propagation varies significantly. These bands were found in both circular and longitudinal muscle strips. Figure 6 shows an example of one region in the longitudinal layer. Of five Ca^{2+} waves that originated from the same pacing site, the first three events (Fig. 6, *A-C*) had an average conduction velocity of 7 mm/s before entering the region of slowed conduction. Conduction slowed by as much as an order of magnitude within the region (*frames 12-17*). The original conduction velocities were then restored once events emerged from the region. The fourth event (Fig. 6*D*) slowed and then stopped in the region where conduction was delayed. The termination of an event within a region of slowed conduction was a common finding (30%

Table 1. *Complex patterns of activity in longitudinal muscle*

Series No.	Sequence
1	AAAABABAAAABCBBBCBCC
2	ACCCCECCDC
3	AAAAABBCCCCCDBEEEE
4	AABAAAABBBBCCCDCEDDCEE
5	AABBCCBCDDCDDEEE
6	AABCCCCDEBCDEE
7	AABBBCCCCDEEEEE

In this example involving spontaneous events from 5 pacing sites ~1 mm apart in direction transverse to long axis of muscle fibers (labeled consecutively A–E), sequences of Ca^{2+} waves are designated according to their sites of origin. Parallel to long axis of muscle fibers, events from all pacemaker locations rapidly spread bidirectionally. In the transverse direction, events from site A consistently swept through site B (but not through site C). Events from site B propagated unidirectionally, sweeping toward site C. All other sites generated events that propagated in both directions transverse to long axis of muscle fibers. In most cases, events from sites B–E did not propagate through adjacent pacemaker locations. The last event of one series was followed by a prolonged delay (30–120 s) before next series was initiated. A similar pattern of activity continued throughout entire 30-min observation period in this preparation.

of 30 sequential events during the experiment associated with Fig. 6). On the other hand, ~10% of excitable events (e.g., Fig. 6E) propagated through the same region without an observable delay.

Wide ranges in conduction velocities in regions where propagation slowed were observed. Propagation velocities varied from a 10-fold decrease (as in Fig. 6) to only a slight delay. Slowed conduction was independent of the direction of travel through the region of delayed conduction (data not shown).

Extent of propagation. In all preparations of isolated circular muscle ($n = 12$), Ca^{2+} waves consistently

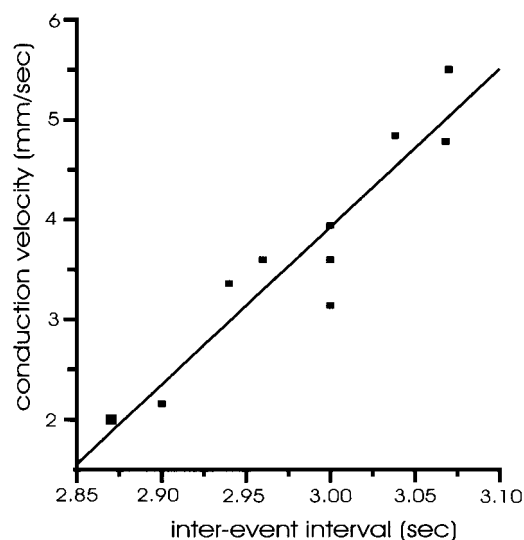


Fig. 5. Conduction velocities increase with increased interevent interval. Conduction velocities transverse to long axis of muscle fibers as a function of time since previous excitation (measured at end of Ca^{2+} wave) and initiation of a new event were measured. All events (■) were generated spontaneously in different regions of a longitudinal tissue segment. The least-squares linear regression ($A\Delta t - B$) superimposed on data has a slope (A) of 16.7 mm/s^2 . B , y -intercept; t , time.

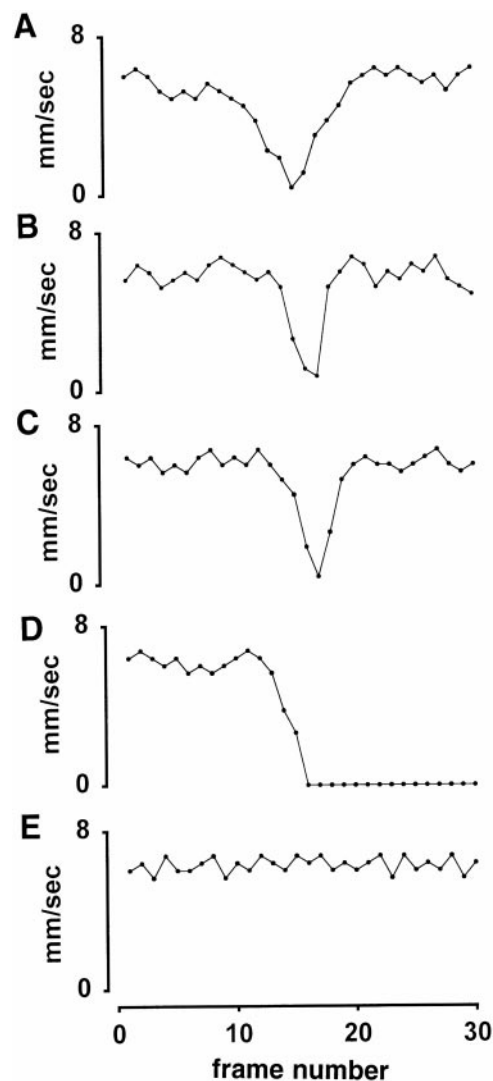


Fig. 6. Region of slowed conduction. Conduction velocities of Ca^{2+} waves were measured on a frame-by-frame basis transverse to long axis of longitudinal muscle fibers in region of slowed conduction. Wave fronts repeatedly approached region at velocity of 5–7 mm/s (A–C). Velocity decreased by up to 1 order of magnitude within region (frames 12–17) before initial conduction velocity was restored on other side of region. D: excitation stopped within region. E: illustration of an event that propagated without delay through same region. A–D show sequential events, and E shows an event that occurred 3 events (as in A–C) after event shown in D.

spread throughout the entire circular layer, even when viewed at low optical magnification (up to 2 cm on a side). This range of spread included any adjacent pacing locations (up to 2) as well as regions excited by these adjacent sites.

In longitudinal muscles, most (but not all) of the Ca^{2+} waves from one pacing site were impeded from propagating through the “domain” (the total region or area covered by an event originating from a single pacing site) of an adjacent pacing site. Propagation generally stopped when events encountered tissue regions recently excited; however, domains were not rigid. Figure 7 shows an example in which two pacemakers (sites A and B in the background image of Fig. 7A) initiated

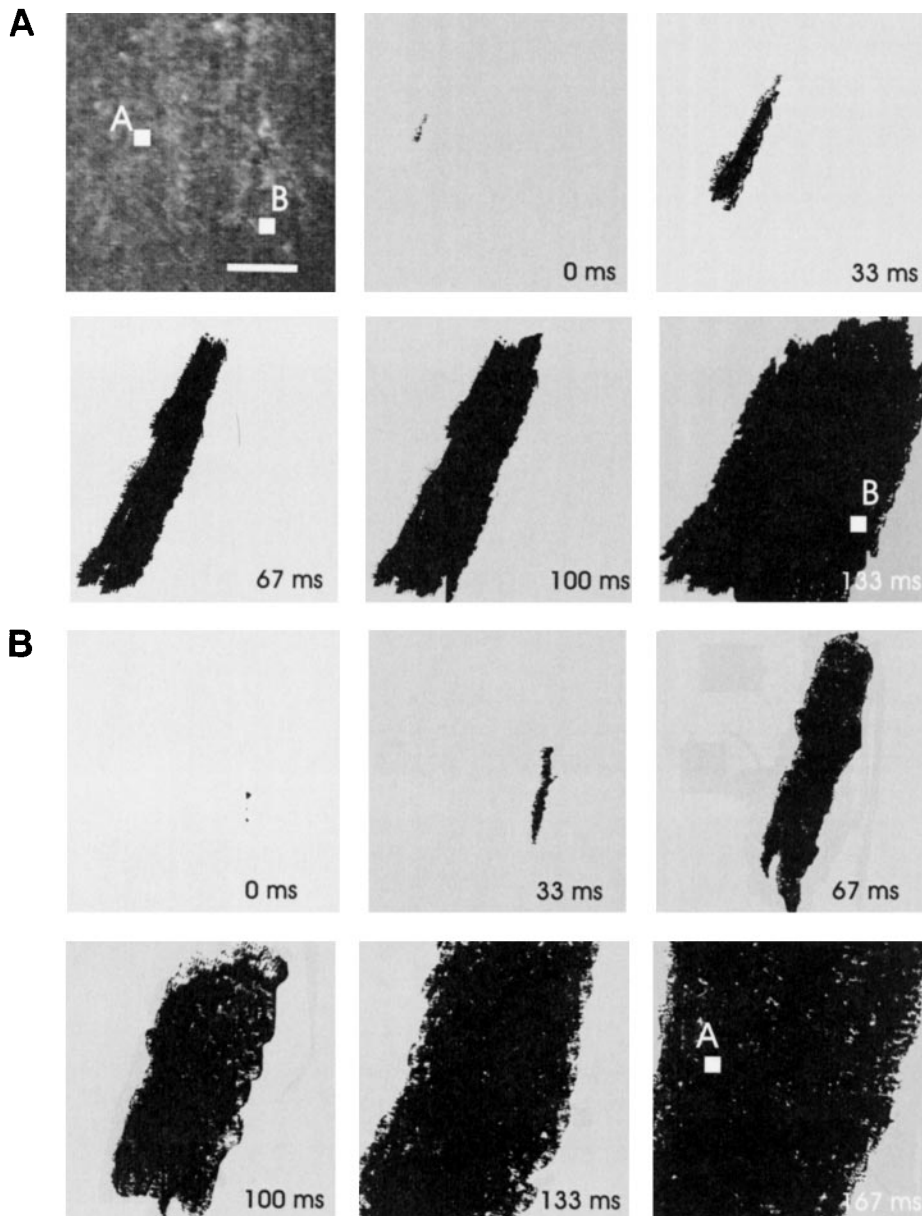


Fig. 7. Propagated Ca^{2+} waves can overlap pacemaker domains. Background image of a sheet of longitudinal muscle with circular muscle removed (*A*, top left) shows location of 2 pacing sites (*A* and *B*). *A*: Ca^{2+} wave that originated at site *A* and propagated across field of view, encompassing site *B* (frame at 133 ms). Subsequent event originated at site *B* and propagated in opposite direction through syncytium to encompass site *A* (*B*). Scale bar = 2 mm

events that swept into each other's domains. The frames in Fig. 7*A* show an event starting at site *A* and sweeping through an active pacing site at site *B* (frame at 133 ms). Figure 7*B* shows the next event emerging from site *B* to sweep through and beyond the pacing site at site *A* (frame at 167 ms). All longitudinal tissues ($n = 14$) demonstrated at least some events that swept into adjacent domains. In some cases in longitudinal muscle, a single Ca^{2+} wave could be seen to sweep through at least three distinct pacing sites.

The frequencies of activation and extent of Ca^{2+} wave propagation produced complex sequences of activity in both longitudinal and circular muscle sheets (see, for example, Fig. 9*B*). It was difficult to predict overall patterns of excitation; however, propagation consistently stopped, and pacing was not observed in recently excited regions. In fact, it was possible to observe "collisions" of actively propagating events. Figure 8

shows an example of two Ca^{2+} waves that were spontaneously initiated at approximately the same time, separated by 3 mm in the direction transverse to the long axis of longitudinal muscle fibers. The two waves of excitation approached each other and then collided (frame at 167 ms). Regions excited as a result of two or more wave fronts that encountered each other generated fluorescence levels that were the same as those generated by propagated events from a single pacemaker site. In other words, there was no summation of fluorescence despite multiple excitatory pathways.

Factors that influence pacing site frequency and location. In the absence of tissue manipulations (see next paragraph), pacing locations appeared to be relatively stable over a time scale of 30 min. Occasionally a site in longitudinal muscle preparations was lost or gained within this period. To test the possibility that neural activity might influence pacemaker activity,

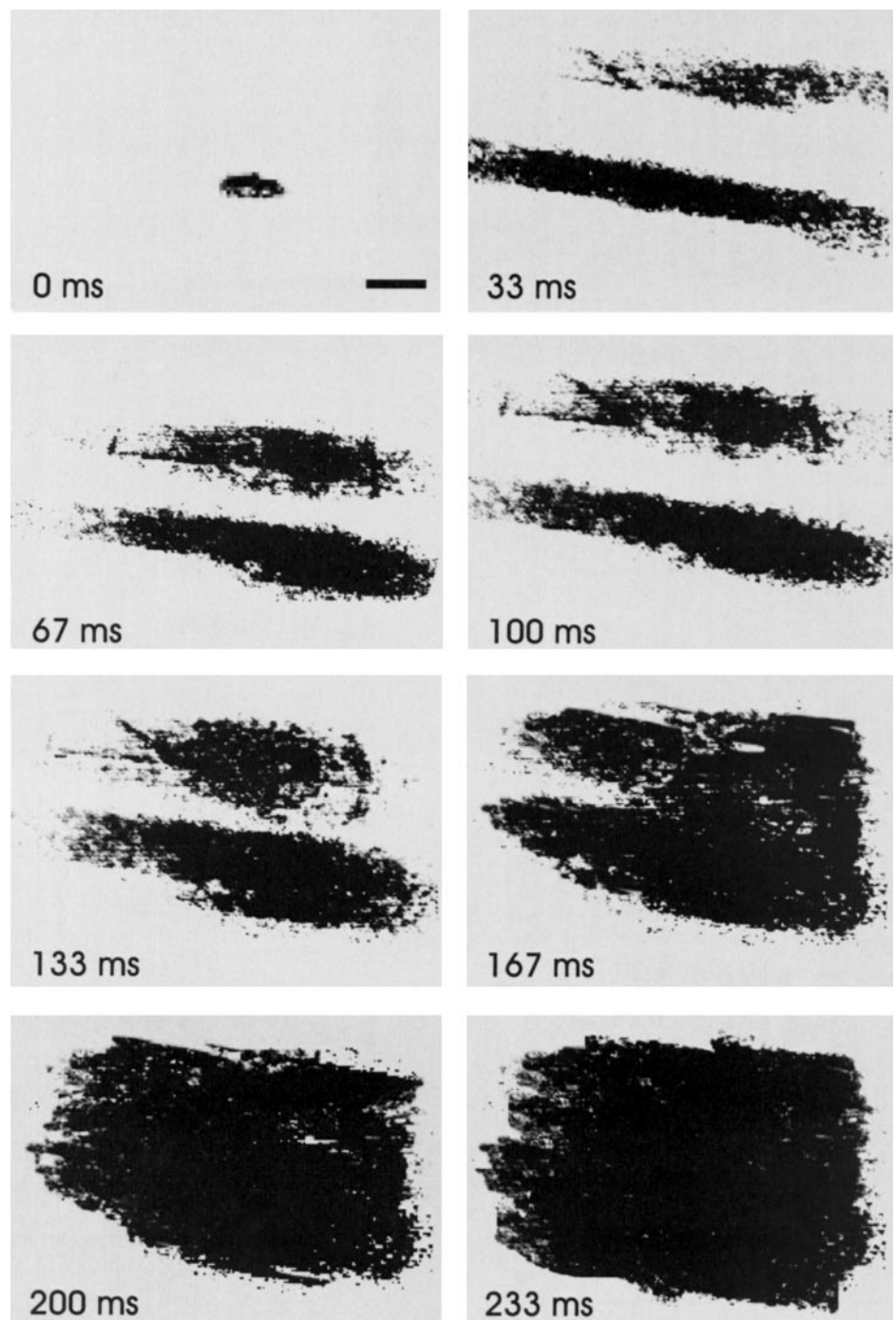


Fig. 8. Collision of 2 Ca^{2+} waves. Contrast-enhanced images show excitation in a sheet of longitudinal muscle viewed from serosal side. Two spatially separate Ca^{2+} waves spontaneously arose nearly simultaneously (0–33 ms). Activity spread rapidly in direction parallel to long axis of muscle fibers and more slowly in transverse direction, resulting in a collision wave front at 133–167 ms. Scale bar = 2 mm.

sheets of longitudinal muscle ($n = 8$) were treated with TTX ($1 \mu\text{M}$; preincubated for 10 min). In 60% of tissues, one or more pacemaker sites that were previously active became quiescent and/or new sites emerged. This turnover in pacemaker sites was somewhat greater than the rate in untreated tissues; however, the overall number of pacemaker sites (average of 5) and spontaneous frequency ($16 \pm 3 \text{ min}^{-1}$) remained approximately the same. In addition, there were no differences in average spontaneous frequencies or patterns of excitation in tissues cold-stored for extended periods (up to 24 h).

It has long been suspected that tissue injury might stimulate or disrupt pacemaker sites in gastrointestinal muscles (18, 19). Experiments were designed to test whether, well-defined, localized injury might alter the frequency or location of pacing activity. Figure 9 shows an example of the effects of local injury created by penetration with a fine microelectrode in a longitudinal muscle preparation. Four pacing sites (locations shown in Fig. 9A) were active before injury (Fig. 9B). Penetration of the tissue by an unfilled glass micropipette (0.2 mm in diameter) caused increased fluorescence in the region around the pipette. Away from the site of injury

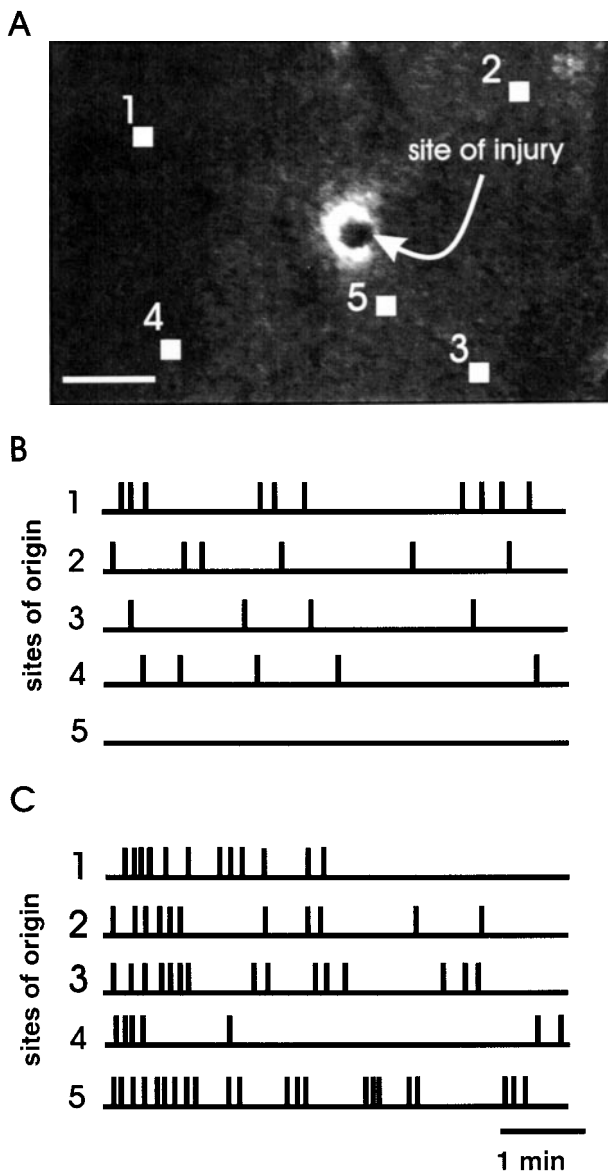


Fig. 9. Patterns of excitation are altered by tissue injury. *A*: locations of 5 pacing sites and site of injury resulting from tissue penetration and immediate withdrawal of a 0.2-mm-diameter unfilled glass micropipette (arrow; image taken immediately after injury). *B*: sequence of spontaneous events from 4 active pacing sites just before injury. Immediately after injury (*C*), there was a burst of activity from all pacemaker sites. Site 5, which was previously quiescent, became active and site 1 became quiescent 2 min after injury. Scale bar = 2 mm.

(>1 mm) there was no influence on membrane potential (on the basis of intracellular recordings), and video images show that the region of elevated $[Ca^{2+}]_i$ was confined to a radius of <2 mm. Immediately after penetration (and withdrawal of the micropipette) a burst of activities from all sites, including a new site within the region of elevated fluorescence (site 5 in Fig. 9), ensued. The new site generated the highest frequency of spontaneous activity (although this was not a consistent finding), and activity from the new site persisted throughout the observation period (30 min). Within 2 min after injury, a previously active site (site 1

in Fig. 9) stopped producing events. No further events were initiated from site 1 throughout the rest of the observation period (>30 min).

It was difficult to predict the specific effects of an injury within a preparation. In 70% of tissues injured by a 0.2-mm glass micropipette, new sites were formed ($n = 14$ injuries in 6 preparations). In 28% of preparations, activity in one or more sites ceased immediately after penetration and additional sites were lost within minutes after injury. An injury created by a much larger (0.4-mm diameter) tungsten electrode on penetration resulted in four of eight sites ceasing initiating events and in the emergence of six new pacing sites to generate activity. New sites appeared up to at least 7 mm away from the site of penetration; however, effects even further away (outside of the field of view) could not be ruled out. Data suggest that syncytial excitation is not governed by single pacemakers but rather results from complex interactions among numerous potential sites.

DISCUSSION

Fluorescence imaging by using Ca^{2+} -sensitive dyes to detect regions of excitation provides an effective technique to examine the dynamics and interactions of activities at the tissue level. Imaging in the gastrointestinal tract has a particular advantage over similar techniques employed, for example, in the heart (20) or brain (11), because propagation velocities are relatively slow and wave fronts can generally be resolved at standard video rates (25–30 frames/s). The present work demonstrates that fluorescence video imaging can be used to assess 1) the origin of tissue activation, 2) the spread of excitation including conduction velocities and the range of propagation of individual events, and 3) alterations in patterns of excitation by factors such as neural blockade and localized injury.

With a single-stage intensified camera, there was insufficient fluorescence (without signal averaging that would result in a loss of temporal resolution) to employ narrow-bandwidth filters to collect paired images for dual-wavelength, calibrated measures of changes in $[Ca^{2+}]_i$. In canine gastric antral tissues, we have previously demonstrated (22) using the ratiometric fluorescent indicator indo 1 that slow waves and contractions are associated with concurrent elevations in $[Ca^{2+}]_i$. In the present study, we have not conclusively shown that increases in fluo 3 fluorescence associated with oscillations during the plateau phase of slow waves in circular muscle and spikes in longitudinal muscle result solely from an increase in $[Ca^{2+}]_i$. These activities might, for example, be influenced by changes in cell volume. Nonetheless, fluorescence video sequences can be used to assess the initiation, spread, and termination of each of these forms of activity at the tissue level.

Resting membrane potentials in circular muscle preparations loaded with fluo 3 in cells near the myenteric border were within the same range of values (-70 ± 4 mV) previously reported by numerous laboratories for preparations not illuminated or loaded with a

fluorescent indicator (1, 5, 12, 37). Similarly, plateau potentials recorded in cells loaded with fluo 3 are in the same range (-31 ± 3 mV) as that for untreated tissues (1, 5). Spontaneous slow-wave frequencies are also consistent with previously reported results (1.6 ± 0.6 min⁻¹) for nonloaded tissues (31). The characteristic waveform of slow waves appears to be unaffected by dye loading, including the presence of oscillations during the plateau phase (Fig. 2C), often seen in tissues taken from more distal regions of the stomach (5, 12, 37). In video sequences, average Ca²⁺ wave propagation velocities were in the same range as that previously reported for slow waves (6.5 ± 4 mm/s transverse and 39 ± 8 mm/s parallel to the long axis of muscle fibers) on the basis of techniques using multiple intracellular microelectrodes (26). Propagation velocities of Ca²⁺ waves in the longitudinal muscle layer are similar to those in circular muscle, suggesting that mechanisms of conduction in the two layers may be similar.

Taken together, these data suggest that dye loading and tissue illumination do not significantly alter the characteristic electrical activities, spontaneous frequencies, or ability of events to propagate through gastric syncytia. On the other hand, tissue penetration by microelectrodes can alter sites of pacemaker activity (Fig. 9). Thus commonly employed intracellular and extracellular techniques using microelectrodes might alter excitation patterns in some preparations.

Fluorescence imaging as a measure of excitation. At the tissue level, previous work has shown that there is a tight correlation between slow-wave depolarization, increases in [Ca²⁺]_i, and the subsequent production of force (22). The present study confirms and extends the correlations between electrical depolarizations and increases in fluorescence to include oscillations in membrane potential during the plateau phase of the slow wave and spikelike depolarizations superimposed atop slow waves in the longitudinal layer. In circular muscle, fluorescent oscillations during the slow wave are spatially confined to the region of elevated [Ca²⁺]_i associated with the slow wave. Except for this constraint, superimposed oscillations originate and propagate as independent events, distinct from the underlying rise in [Ca²⁺]_i. The similarity in range of conduction velocities compared with slow-wave propagation and the presence of collisions between oscillations suggest that the excitability mechanisms associated with oscillations are similar to those of other excitable events in smooth muscle. Their role may be to enhance the strength of contractions during slow waves by stimulating additional transient Ca²⁺ entry without elevating [Ca²⁺]_i in a sustained fashion, which might be harmful to the cell.

In longitudinal muscle preparations, the underlying rhythmicity is similar to so-called myenteric potential oscillations that have been observed in canine distal colon (34). Slow waves recorded by electrophysiological techniques were consistently associated with concurrent Ca²⁺ waves. On the other hand, superimposed "spikes" or brief fluctuations (<0.5 s) in fluorescence observed in video sequences were not always associated

with spikelike depolarizations or action potentials recorded intracellularly. It has previously been suggested, on the basis of microelectrode recordings, that these action potentials do not propagate in gastric and duodenal tissues (33). Video sequences indicate that fluorescence transients associated with spikes do have discrete sites of origin and propagate over short distances. Similar to fluorescence oscillations in the circular layer, they are confined to a region of elevated [Ca²⁺]_i dictated by underlying activity. However, unlike oscillations, spikes in the longitudinal layer were not observed in all cells within a region of elevated fluorescence (superimposed atop the Ca²⁺ transient) by electrophysiological techniques. These observations are consistent with the notion that the spread of high-frequency components of electrical activity might be strongly attenuated by the syncytial nature of the tissue (24).

Origin of activation. It has previously been suggested that gastric (28) and other smooth muscles (13, 15, 16) contain hot spots or preferred locations where excitable events are initiated. Fluorescence video images verify that this is the case for both the longitudinal and circular muscle layers in the stomach. It appears that both layers contain numerous "potential" pacing sites, because new sites can readily be induced after a localized injury. However, during spontaneous activity, a small number of sites dominate pacemaker activity during all forms of activation within the two muscle layers. To within the spatial and temporal resolution of video images (revealing small muscle bundles), events repeatedly initiate from these same sites, even when events from other sites are interspersed (Fig. 4).

In cross-sectional muscle preparations, Ca²⁺ transients associated with electrical slow waves consistently originate from the circular-longitudinal muscle boundary, initiating waves of excitation that simultaneously propagate parallel and transverse to the long axis of circular fibers (Fig. 3). The locations of the sites of origin are consistent with the notion promoted by a number of laboratories that interstitial cells of Cajal associated with the myenteric plexus region may serve the role of the pacemaker in the stomach and other intestinal muscles (9, 29, 30).

Longitudinal tissues contain more active pacing sites than similarly sized circular tissues. It is not clear whether the reason for this is the higher intrinsic rate of activity in the longitudinal layer or that the extent of propagation from each site is more confined. There is likely an interplay involving the number of pacemakers, intrinsic frequencies, and extent of propagation around each site. In some cases, there is clearly a coordination or synchronization among longitudinal pacemakers that can produce complex patterns of activity lasting up to at least 1 h (Table 1). TTX (1 μM) can partially disrupt these patterns, although the overall frequency of excitation in gastric tissues remains unchanged. This suggests some form of neural modulation; however, the continued presence of patterned activity suggests that at least some aspects of the coordination of activation are governed by non-TTX-dependent mechanisms.

Propagation of excitation. Historically, it has been suggested that pacemakers control a region or domain within a tissue segment (32). In circular muscles, all Ca^{2+} waves spread throughout the entire field of view including any nearby pacing sites. Thus it is likely that the size of any domain in circular muscle includes the entire circumference of the organ along the long axis of circular muscle fibers and segments greater than the field of view (2 cm under low magnification) along the length of the stomach. In contrast, in longitudinal muscles (e.g., Fig. 2), most (but not all) events, from a single pacing site, did not propagate through adjacent domains. Propagation usually stopped when events encountered regions recently excited by adjacent pacemakers. Regions excited by the collision of two events (e.g., Fig. 8) were not distinguishable from unitary events in the same region. However, rigid pacing domains were not observed consistently (e.g., Fig. 7). All longitudinal tissues demonstrated at least some events that swept into adjacent pacemaker regions including pacing sites. This loose regional influence of domains may be a part of the segmental level of control in gastrointestinal muscles.

Previously, it was assumed that propagation in gastrointestinal smooth muscles proceeds at uniform rates parallel and transverse to the long axis of muscle fibers (27). Video sequences of the spread of Ca^{2+} waves demonstrate that this is not the case. There appears to be a basal, more rapid rate of conduction (6–10 mm/s transverse to muscle fibers) in most regions of a tissue, with spatially well-defined areas of slowed conduction. Slowed conduction generally occurs repeatedly at the same anatomical sites (see Fig. 6). The degree of slowing varies from event to event at a given site, and in some cases events were observed to proceed without slowing through these sites (e.g., Fig. 6E). These data suggest that there may be a mechanism to regulate the overall rate of conduction in a syncytium by controlling conduction through specific regions within a tissue. The electrophysiological mechanism or mechanisms that cause delayed conduction (e.g., reduced membrane resistance, elevated cell-to-cell junctional resistance) have not been determined in this study. It is possible that regions of delayed conduction may be associated with septal structures or other morphological features (6, 38).

Regions of slowed conduction may also play an important role in regulating the extent of propagation. When viewed in terms of elapsed time (as opposed to conduction velocities), an event can spend 25–50% or more of its overall lifetime in regions of delayed conduction (see Fig. 6). Thus not only might these regions influence rates of conduction, they can also be the most likely locations for event termination. This may provide an opportunity for influencing the extent and rate of propagation (neural or otherwise) by directly modulating these specific locations without controlling the entire syncytium.

It has previously been shown (26) that conduction velocities in circular muscle depend on the "interevent" interval (the time since a region was last excited). The

present study (e.g., Fig. 5) furthers this concept to spontaneously initiated events in two-dimensional sheets of longitudinal muscle. Conduction velocity (transverse to muscle fibers) increases with longer interevent intervals. This property of the syncytium may contribute to the regulation of activation within a syncytium by limiting rates of conduction into regions recently excited. This might be particularly important in the longitudinal muscle layer where there is a greater density of distinct regions influenced by different pacing sites.

Although fluorescence imaging reveals a spatially heterogeneous range of conduction velocities, when viewed macroscopically, average conduction velocities are similar to those measured with multiple electrodes (28). Video data can be used to augment electrophysiological results, although some care must be exercised when comparing fluorescence imaging results with those obtained by traditional microelectrode techniques. For example, in longitudinal muscles, Ca^{2+} waves and spikes generally do not sweep throughout an entire tissue (at the scale of a few millimeters), so individual electrodes do not record all events in a given field of view viewed within video sequences. Thus measurements of frequencies must be confined to a specific location within the tissue to produce results comparable to those obtained by microelectrode-based techniques. In addition, in longitudinal muscles the most rapid fluorescence transients (see Fig. 2) do not always result in a "spike" potential in individual cells recorded electrophysiologically even though transients can be seen to sweep through the region of a microelectrode recording.

Alterations in tissue excitability. In the antrum, neural blockade generated only minor shifts in pacing locations, with no effect on frequency. These data are in sharp contrast to recently reported results (35) from guinea pig colon where the enteric nervous system appears to play a major role in regulating both the number of pacing sites and the frequency of activity at each site. Differences may be due to different functions within these regions of the gastrointestinal tract. Locally initiated peristaltic contractions in the colon appear to be under strong neural control, whereas the initiation of contractions that generally sweep through the antral region of the stomach appears to be largely independent of neural input.

For some time, there has been speculation that injury might generate an effect on pacemaker activity in the stomach (18, 19). Fluorescence imaging clearly shows that injury can induce new pacemaker activity in the vicinity of the injury site. However, the effects of injury were confined neither to the induction of new sites nor to the region of injury. Pacemaker sites can be lost or gained after localized injury. In most tissues, both processes were observed: some pacemaker sites were lost while others were gained within a short period after injury (Fig. 9). Pacemaker sites (lost or gained) can be near the injury (i.e., near the site of elevated fluorescence) or at distances up to at least several millimeters away from the injury.

Because of collateral propagation around a localized injury site, there is a minimal effect on the time of arrival of activation, even a short distance away (<1 mm) from the site of a localized injury. The physiological consequences of a confined injury may be less associated with disrupting conduction pathways. More significantly, injury appears to alter the initiation and sequence of excitation throughout the entire syncytium.

In summary, the origin, propagation, and extinction of activity can generate complex patterns of excitation in three-dimensional gastrointestinal syncytia. Ca^{2+} transients associated with slow waves, oscillations, and spikes are confined both morphologically and functionally to tissue regions; however, each contributes uniquely to overall tissue excitation. Even small tissue segments with few pacing sites can generate a rich repertoire of activity.

This grant was supported by National Institute of Diabetes and Digestive and Kidney Diseases grant DK-32176.

Address for reprint requests and other correspondence: N. G. Publicover, Biomedical Engineering Program, Dept. of Physiology and Cell Biology, Univ. of Nevada School of Medicine, Reno, NV 89557 (E-mail: nelson@unr.edu).

Received 3 November 1998; accepted in final form 14 May 1999.

REFERENCES

- Bauer, A. J., N. G. Publicover, and K. M. Sanders. Origin and spread of slow waves in canine gastric antral circular muscle. *Am. J. Physiol.* 249 (*Gastrointest. Liver Physiol.* 12): G800–G806, 1985.
- Burnstock, G., and C. L. Prosser. Conduction in smooth muscles: comparative electrical properties. *Am. J. Physiol.* 199: 553–559, 1960.
- Carl, A., H. K. Lee, and K. M. Sanders. Regulation of ion channels in smooth muscles by calcium. *Am. J. Physiol.* 271 (*Cell Physiol.* 40): C9–C34, 1996.
- Code, C. F., J. H. Szurszewski, and K. A. Kelly. A concept of motor control by the pacesetter potential in the stomach and small bowel. *Nippon Heikatsukin Gakkai Zasshi* 6: 67–68, 1970.
- El-Sharkawy, T. Y., K. G. Morgan, and J. H. Szurszewski. Intracellular electrical activity of canine and human gastric smooth muscle. *J. Physiol. (Lond.)* 279: 291–307, 1978.
- Faussone-Pellegrini, M. S., D. Pantalone, and C. Cortesini. An ultrastructural study of the interstitial cells of Cajal of the human stomach. *J. Submicrosc. Cytol. Pathol.* 21: 439–460, 1989.
- Gabella, G. On the ultrastructure of the enteric nerve ganglia. *Scand. J. Gastroenterol. Suppl.* 71: 15–25, 1982.
- Gryniewicz, G., M. Poenie, and R. Y. Tsien. A new generation of Ca^{2+} indicators with greatly improved fluorescence properties. *J. Biol. Chem.* 260: 3440–3450, 1985.
- Hagger, R., C. Finlayson, I. Jeffrey, and D. Kumar. Role of the interstitial cells of Cajal in the control of gut motility. *Br. J. Surg.* 84: 445–450, 1997.
- Huizinga, J. D., L. W. Liu, M. G. Blennerhassett, L. Thuneberg, and A. Molleman. Intercellular communication in smooth muscle. *Experientia* 48: 932–941, 1992.
- Jaffe, D. B., and T. H. Brown. Confocal imaging of dendritic Ca^{2+} transients in hippocampal brain slices during simultaneous current- and voltage-clamp recording. *Microsc. Res. Tech.* 29: 279–289, 1994.
- Kelly, K. A., and C. F. Code. Canine gastric pacemaker. *Am. J. Physiol.* 220: 112–118, 1971.
- Lammers, W. J., A. al-Kays, S. Singh, K. Arafat, and T. Y. el-Sharkawy. Multielectrode mapping of slow-wave activity in the isolated rabbit duodenum. *J. Appl. Physiol.* 74: 1454–1461, 1993.
- Lammers, W. J., K. Arafat, A. el-Kays, and T. Y. el-Sharkawy. Spatial and temporal variations in local spike propagation in the myometrium of the 17-day pregnant rat. *Am. J. Physiol.* 267 (*Cell Physiol.* 36): C1210–C1223, 1994.
- Lammers, W. J., A. el-Kays, G. W. Manfield, K. Arafat, and T. Y. el-Sharkawy. Disturbances in the propagation of the slow wave during acute local ischaemia in the feline small intestine. *Eur. J. Gastroenterol. Hepatol.* 9: 381–388, 1997.
- Lammers, W. J., B. Stephen, K. Arafat, and G. W. Manfield. High resolution electrical mapping in the gastrointestinal system: initial results. *Neurogastroenterol. Motil.* 8: 207–216, 1996.
- Makhlof, G. M., and K. S. Murthy. Signal transduction in gastrointestinal smooth muscle. *Cell. Signal.* 9: 269–276, 1997.
- Malagelada, J. R. Gastric emptying disorders. Clinical significance and treatment. *Drugs* 24: 353–359, 1982.
- Malagelada, J. R. Gastric motility disorders and their clinical implications. *Scand. J. Gastroenterol. Suppl.* 165: 29–34, 1989.
- Minamikawa, T., S. H. Cody, and D. A. Williams. In situ visualization of spontaneous calcium waves within perfused whole rat heart by confocal imaging. *Am. J. Physiol.* 272 (*Heart Circ. Physiol.* 41): H236–H243, 1997.
- Nagai, T., and C. Prosser. Patterns of conduction in smooth muscle. *Am. J. Physiol.* 204: 910–914, 1963.
- Ozaki, H., R. J. Stevens, D. P. Blondfield, N. G. Publicover, and K. M. Sanders. Simultaneous measurement of membrane potential, cytosolic Ca^{2+} , and tension in intact smooth muscles. *Am. J. Physiol.* 260 (*Cell Physiol.* 29): C917–C925, 1991.
- Prosser, C., G. Burnstock, and J. Kahn. Conduction in smooth muscle: comparative structural properties. *Am. J. Physiol.* 199: 545–552, 1960.
- Publicover, N. G., and K. M. Sanders. Are relaxation oscillators an appropriate model of gastrointestinal electrical activity? *Am. J. Physiol.* 256 (*Gastrointest. Liver Physiol.* 19): G265–G274, 1989.
- Publicover, N. G., and K. M. Sanders. Effects of frequency on the wave form of propagated slow waves in canine gastric antral muscle. *J. Physiol. (Lond.)* 371: 179–189, 1986.
- Publicover, N. G., and K. M. Sanders. Myogenic regulation of propagation in gastric smooth muscle. *Am. J. Physiol.* 248 (*Gastrointest. Liver Physiol.* 11): G512–G520, 1985.
- Publicover, N. G., and K. M. Sanders. Regulation of slow wave propagation in the stomach. *Proc. West. Pharmacol. Soc.* 27: 119–122, 1984.
- Publicover, N. G., and K. M. Sanders. A technique to locate the pacemaker in smooth muscles. *J. Appl. Physiol.* 57: 1586–1590, 1984.
- Rumessen, J. J., and L. Thuneberg. Pacemaker cells in the gastrointestinal tract: interstitial cells of Cajal. *Scand. J. Gastroenterol. Suppl.* 216: 82–94, 1996.
- Sanders, K. M. A case for interstitial cells of Cajal as pacemakers and mediators of neurotransmission in the gastrointestinal tract. *Gastroenterology* 111: 492–515, 1996.
- Sanders, K. M., and A. J. Bauer. Ethyl alcohol interferes with excitation-contraction mechanisms of canine antral muscle. *Am. J. Physiol.* 242 (*Gastrointest. Liver Physiol.* 5): G222–G230, 1982.
- Sarna, S. K., K. L. Bowes, and E. E. Daniel. Gastric pacemakers. *Gastroenterology* 70: 226–231, 1976.
- Sarna, S. K., E. E. Daniel, and Y. J. Kingma. Simulation of the electric-control activity of the stomach by an array of relaxation oscillators. *Am. J. Dig. Dis.* 17: 299–310, 1972.
- Smith, T. K., J. B. Reed, and K. M. Sanders. Interaction of two electrical pacemakers in muscularis of canine proximal colon. *Am. J. Physiol.* 252 (*Cell Physiol.* 21): C290–C299, 1987.
- Stevens, R. J., N. G. Publicover, and T. K. Smith. Induction and organization of Ca^{2+} waves by enteric neural reflexes. *Nature*. 399: 62–66, 1999.
- Thuneberg, L. Interstitial cells of Cajal: intestinal pacemaker cells? *Adv. Anat. Embryol. Cell Biol.* 71: 1–130, 1982.
- Vogalis, F., N. G. Publicover, J. R. Hume, and K. M. Sanders. Relationship between calcium current and cytosolic calcium in canine gastric smooth muscle cells. *Am. J. Physiol.* 260 (*Cell Physiol.* 29): C1012–C1018, 1991.
- Ward, S. M., and K. M. Sanders. Pacemaker activity in septal structures of canine colonic circular muscle. *Am. J. Physiol.* 259 (*Gastrointest. Liver Physiol.* 22): G264–G273, 1990.